

Sum Throughput Maximization in Multi-BD Symbiotic Radio NOMA Network Assisted by Active-STAR-RIS

Rahman Saadat Yeganeh¹, Mohammad Javad Omid^{1,2}, Farshad Zeinali³,
Mohammad Robot Mili⁴, and Mohammad Ghavami⁵, *Senior Member, IEEE*

Abstract

In this paper, we employ active simultaneously transmitting and reflecting reconfigurable intelligent surface (ASRIS) to aid in establishing and enhancing communication within a commensal symbiotic radio (CSR) network. Unlike traditional RIS, ASRIS not only ensures coverage in an omni directional manner but also amplifies received signals, consequently elevating overall network performance. In the first phase, base station (BS) with active massive MIMO antennas, send ambient signal to SBDs. In the first phase, the BS transmits ambient signals to the symbiotic backscatter devices (SBDs), and after harvesting the energy and modulating their information onto the signal carrier, the SBDs send Backscatter signals back to the BS. In this scheme, we employ the Backscatter Relay system to facilitate the transmission of information from the SBDs to the symbiotic User Equipments (SUEs) with the assistance of the BS. In the second phase, the BS transmits information signals to the SUEs after eliminating interference using the Successive Interference Cancellation (SIC) method. ASRIS is employed to establish communication among SUEs lacking a line of sight (LoS) and to amplify power signals for SUEs with a LoS connection to the BS. It is worth noting that we use NOMA

¹Department of Electrical and Computer Engineering, Isfahan University of Technology, Isfahan 84156-83111, IRAN (emails: r.saadat@ec.iut.ac.ir, omidi@iut.ac.ir).

²Department of Electronics and Communication Engineering, Kuwait College of Science and Technology (KCST), Doha 35003, Kuwait

³Electrical and Electronic Engineering Department, Tarbiat Modares University, Tehran, Iran, Postal Code: 14115 (email: zeinali@modares.ac.ir).

⁴Mohammad Robot Mili is with the Pasargad Institute for Advanced Innovative Solutions (PIAIS), Tehran, Iran (E-mail: Mohammad.Robotmili@gmail.com).

⁵Electrical and Electronic Engineering Department, London South Bank University, London SE1 0AA, U.K.(email: ghavamim@lsbu.ac.uk).

for multiple access in all network. The main goal of this paper is to maximize the sum throughput between all users. To achieve this, we formulate an optimization problem with variables including active beamforming coefficients at the BS and ASRIS, as well as the phase adjustments of ASRIS and scheduling parameters between the first and second phases. To model this optimization problem, we employ three deep reinforcement learning (DRL) methods, namely PPO, TD3, and A3C. Finally, the mentioned methods are simulated and compared with each other.

Index Terms

Symbiotic radio, Active STAR-RIS, Sum throughput maximization, IoT, NOMA.

I. INTRODUCTION

A. Background

Future networks such as B5G and 6G must be capable of covering billions of internet-of-things (IoT) and wireless devices [1]. The IoT stands out as a pivotal technology in shaping the future of wireless communications, embracing a diverse range of applications, including smart transportation, smart homes, smart grids, and smart agriculture [2]. However, the extensive deployment of IoT devices faces two critical challenges: energy efficiency and spectrum scarcity issues [3]–[5]. The spectrum scarcity challenge arises from the limited availability of spectrum resources for IoT applications, as a substantial portion has already been allocated to various radio systems. This constraint necessitates the urgent resolution of these challenges to optimize spectrum utilization. Additionally, the energy efficiency issue presents a significant obstacle, given the high cost associated with regularly charging devices or replacing batteries [6].

The envisaged solution we propose to overcome the mentioned challenges involves the use of Symbiotic Radio (SR) and Reconfigurable Intelligent Surfaces (RIS).

SR stands out as an innovative technology that not only preserves the merits of prior systems like cognitive radio [7]–[9] and ambient backscatter communication (AmBC) [10], [11] but also addresses and eliminates their drawbacks. It currently ranks among the captivating subjects in both scientific and industrial domains [12], [13]. The SR network can be classified into parasitic SR (PSR) and commensal SR (CSR) based on the relationship between the symbol periods of the symbiotic backscatter devices (SBDs) and the BS [11], [14]. In PSR setup, SBDs can exchange information at a high rate, but it also suffers from interference between the signals of SBDs and BS in the receiver, necessitating complex interference cancellation techniques.

Furthermore, PSR requires synchronization between the BS, BD, and receiver. On the other hand, CSR is suitable for IoT networks with low data rates, and addresses the drawbacks of the PSR system. By reducing interference between different network components, the receiver can perform joint decoding of information from both the BS and SBDs, enabled by transmit collaboration between them [7], [15]. In the article [16], SR network is presented, implemented in CSR form, particularly tailored for the multiple backscatter device scenario. The primary goal within this framework is to reduce energy consumption, and a method for optimal resource allocation, named Timing-SR, has been introduced as well. Also, the article [14], proposes a novel SR technique for passive IoT devices. This approach involves integrating a BD with a primary communication system, and designing a primary transmitter and receiver to optimize both the primary and BD transmissions. The decoding strategy used in the receiver is based on SIC.

On the other hand, RIS is a new technology composed of two-dimensional surface that can reduce the need for expensive BS antennas with complex hardware in the network and provide complete coverage over a specific area. The initial type of these surfaces only had the capability to reflect signals in one direction [17], and due to inadequate coverage, a more advanced type called simultaneously transmitting and reflecting RIS (STAR-RIS) was introduced in subsequent designs [18], [19]. STAR-RISs are equipped with a large number of low-cost passive elements whose transmission and reflection (T&R) coefficients can be controlled. In the paper [20], a STAR-RIS assisted multiple-input multiple-output (MIMO) system, in which the sum-rate maximization problem was investigated in both unicasting and broadcasting signal models. Also, in the [21], an investigation into the secrecy performance of STAR-RIS-assisted Non-Orthogonal Multiple Access (NOMA) networks took place.

It is worth emphasizing that utilizing STAR-RIS in passive mode necessitates a substantial number of elements on its surface to attain optimal operational gains, resulting in its enlargement. This presents a formidable challenge to the expansion of these systems. As a result, recent research endeavors have introduced the concept of ASRIS to deftly tackle and resolve this issue [22]. In [23], the proposition of active RISs and the investigation of joint optimization for reflecting phase shift and receive beamforming were introduced. Subsequently, [24] presented a validated signal model for active RISs. Nevertheless, there exists a current gap in research contributions concerning the modeling and performance analysis of active STAR-RISs. In the article [22], a hardware model is introduced for active STAR-RISs incorporating both coupled

and independent T&R phase-shifts. More precisely, this paper demonstrates the utilization of reflection-type amplifiers and quadrature hybrid couplers to achieve amplification of the T&R coefficients.

SR systems typically suffers from the poor system performance owing to the limited communication efficiency of backscattering devices. In an effort to overcome this bottleneck, RIS-enabled SR transmission emerges as a promising technology, demonstrating potential for improved spectrum and energy efficiencies. Due to the abundant advantages of these two subjects and their combination, numerous articles, such as [25]–[27], have been presented in this field. In most current works, RIS deployed in SR systems was predominantly limited to reflection-only RIS. Under these configurations, Primary and Secondary Users are required to be stationed on one side of the RIS, a setup that may lack flexibility for practical network deployment. In the article [28], a passive STAR-RIS empowered transmission scheme for SR systems is presented. The STAR-RIS is utilized to transmit signals from the BS to reflection and transmission users. The authors focused on minimizing the transmit power of the BS by designing the active beamforming and simultaneous reflection and transmission coefficients under the practical phase correlation constraint.

To efficiently accommodate a significant number of devices in SR networks, it is crucial to design the network to support multiple SBDs. However, challenges, including potential user interference with improperly designed multiple access schemes, may arise. To address this, methods like NOMA are employed to prevent such interferences [29]–[31].

In this paper, we propose a network based on the CSR structure, where the BS initially transmits signals to the SBDs on one side using Massive MIMO antennas. SBDs modulate their information onto the received signal carrier. Given the far distance of the passive IoT devices (SBDs) from SUEs, we utilize Backscatter Relay by the BS to transmit the information to SUEs located on the opposite side of the BS [32]. In this system, we incorporate an ASRIS to amplify signals and transmit them to SUEs without a line of sight (LOS) to the BS. In all transmission schemes, the method for multiple access is NOMA. In the assumed system, the objective is to maximize the sum throughput among all users.

The major contributions of this paper are summarized as follows:

- First, we implement an innovative, comprehensive and practical system model where multiple users actively (SUEs) and passively (SBDs) engage in the exchange of diverse information within the network. The configuration employs a CSR setup, wherein the BS

dispatches ambient signals to SBDs using a NOMA approach. Subsequently, SBDs harvest wireless energy from these signals, modulating their own information onto the carrier, and then transmitting Backscatter signals back to the BS. Assisted by ASRIS, the BS efficiently relays this information to SUEs situated in reflection and transmission regions of ASRIS, with LOS and non-LOS link to the BS, respectively.

- Second, to achieve optimal resource allocation in this system, we formulate an optimization problem focused on maximizing the sum information throughput among all users. With the aim of achieving this objective, we define variables in the problem, including active beamforming vector variables in two phases: transmitting signals to SBDs and delivering desired information to SUEs by the BS. We also consider a schedule for the first and second phases and determine the amplifier gain and phase variables for ASRIS. In this endeavor, we impose QoS constraints to ensure a minimum rate for each SBD and SUE. Additionally, constraints related to SIC are incorporated for all transmitted signals from users.
- Third, SBDs can harvest the required energy from ambient waves whenever they have information to transmit. They can send their information to the intended destination without causing interference by utilizing NOMA. Due to the considerable distance between SBDs and SUEs, direct information transmission to SUEs is not feasible. To address this issue, we leverage the power of active Massive MIMO antennas at the BS. After eliminating interference using SIC, each of the signals from SBDs is directed towards the respective SUE. Additionally, the signal modeling in ASRIS is thoroughly examined in this scheme and is incorporated into the overall design.
- Finally, to solve this non-convex problem, we employ deep reinforcement learning (DRL) methods. Three innovative approaches, namely proximal policy optimization (PPO), twin-delayed deep deterministic policy gradient (TD3), and asynchronous advantage actor critic (A3C), each exhibiting distinctive features, were explored. These algorithms are employed to model the problem, and a comprehensive comparison of all simulated methods is conducted under varying conditions.

This paper is structured as follows. In Section II, we present the proposed system model for the ASRIS assisted by the CSR system. Section III focuses on the sum throughput maximization problem. In Section IV, we investigate some Deep Reinforcement Learning (DRL) methods, namely PPO, TD3 and A3C. In Section V, the mentioned methods are modeled and simulated,

followed by a comparison with each other. Finally, in Section VI, we summarize our conclusions and discuss future work.

Notations: $\langle a, b \rangle$ denotes the inner product of a and b , $Tr(\mathbf{A})$, \mathbf{A}^H , \mathbf{A}^T , $\|\mathbf{A}\|$ denote the trace, conjugate transpose, transpose, and norm of the matrix \mathbf{A} , respectively. The positive semi-definite was denoted as $\mathbf{A} \succeq 0$ and ∇ shows the gradient operator.

II. SYSTEM MODEL AND PROBLEM FORMULATION

As illustrated the system model in Fig. 1, the symbiotic radio (SR) system contains the BS equipped with N massive mimo antennas, one ASRIS with M active elements, I -SUEs in transmission and reflection space of ASRIS and I -SBDs with single antenna are considered.

In this structure, the SBDs is positioned at a long distance from the SUEs (relative to the wavelength of the network's operating frequency). Moreover, as the SBDs is a passive device and lacks the capability to transmit information over long distances, it cannot establish a direct backscatter communication link with the SUEs. Therefore, to establish communication, we need to use the cooperative relay structure. An appropriate idea for this is to use the BS capabilities, which is located in the center of the cell and can receive and amplify the SBDs signal. This amplified signal reaches the SUEs through a direct link and with the help of active ASRIS. As a result, the communication between SBDs and SUEs is established through the cooperation of BS and ASRIS. This method significantly increases the range and quality of communication.

In this section, we analyze the communication between the SBDs, BS, ASRIS, and SUEs. The BS establishes a direct communication link with SUE_j in reflection space of ASRIS, while there is no direct link between BS and SUE_j in transmission space of ASRIS.

A. System Model of The Active STAR-RIS

The STAR-RISs are advanced devices that enable independent control of the transmitted and reflected signals. Specifically, the signal incident upon the m th element of the ASRIS is denoted by s_m , where $m \in \mathcal{M} \triangleq \{1, 2, \dots, M\}$. The m th element can adjust the amplitude and phase of the incident signal during transmission and reflection, resulting in transmitted and reflected signals given by $(\sqrt{\beta_m^t} e^{j\theta_m^t}) s_m$ and $(\sqrt{\beta_m^r} e^{j\theta_m^r}) s_m$, respectively. Here, β_m^t and θ_m^t represent the amplitude and phase shift adjustments made by the m th element during transmission, while

β_m^r and θ_m^r represent the corresponding adjustments during reflection. The signals transmitted and reflected by each element of the SRIS can be accurately modeled with this approach [33].

$$t_m = \left(\sqrt{\beta_m^t} e^{j\theta_m^t} \right) s_m, \quad \forall m \in \mathcal{M} \quad (1)$$

$$r_m = \left(\sqrt{\beta_m^r} e^{j\theta_m^r} \right) s_m, \quad \forall m \in \mathcal{M} \quad (2)$$

In the passive structure for the SRIS, the energy conservation law requires that the energy of the incident signal equals the sum of the energies of the transmitted and reflected signals, i.e., $|s_m|^2 = |t_m|^2 + |r_m|^2$ for all $m \in \mathcal{M}$. This means that the amplitude of the transmission and reflection coefficients, are coupled, and hence must satisfy $\beta_m^t + \beta_m^r = 1$. In this paper, in the proposed ASRIS each element operates in simultaneous transmission and reflection mode (T&R mode), which is more general than either full transmission mode (T mode) or full reflection mode (R mode) [18], [34]. As a result, we adopt the operating protocol for the ASRIS known as energy splitting (ES), where all elements of the ASRIS are assumed to operate in T&R mode. The ES mode provides more degrees of freedom for optimizing the network, but it also increases the communication overhead between the BS and ASRIS [34]. In order to reduce complexity and provide greater clarity, we propose a simplified equal energy splitting protocol in our initial attempt [35]. This protocol involves setting $\beta_m^t = \beta_m^r = \frac{p_{ASRIS}}{2}$ in both transmission and reflection modes, where p_{ASRIS} is the constant power in the transmission and reflection modes.

For ease of expression, we define the transmission (when $l = t$) or reflection (when $l = r$) beamforming vector as $\mathbf{R}_l = [\sqrt{\beta_1^l} e^{j\theta_1^l}, \sqrt{\beta_2^l} e^{j\theta_2^l}, \dots, \sqrt{\beta_M^l} e^{j\theta_M^l}]^H \in \mathbb{C}^{M \times 1}$, and let $\Theta_l = \text{diag}(\mathbf{R}_l^H) \in \mathbb{C}^{M \times M}$ be the corresponding diagonal beamforming matrix of ASRIS.

B. Problem Formulation

We propose the implementation of a commensal symbiotic radio (CSR) as the considered structure for the symbiotic radio network. In this configuration, the BS transmits K symbols (where $k = 1, 2, \dots, K$ and $K \gg 1$) for every SBD's data symbol. This means that the duration of each symbol transmitted by SBD is equal to K times of the duration of symbol transmission by BS ($T_{SBD} = KT_{BS}$). With this CSR design, we ensures that the SBDs and BS signals do not interfere with each other at the destination.

In the proposed CSR network, *in the first phase*, the BS transmitted the known signal $s_k(t)$ to SBD_i through the complex channel $\mathbf{h}_{1i}^H \in \mathbb{C}^{1 \times N}$. This transmission is achieved using the

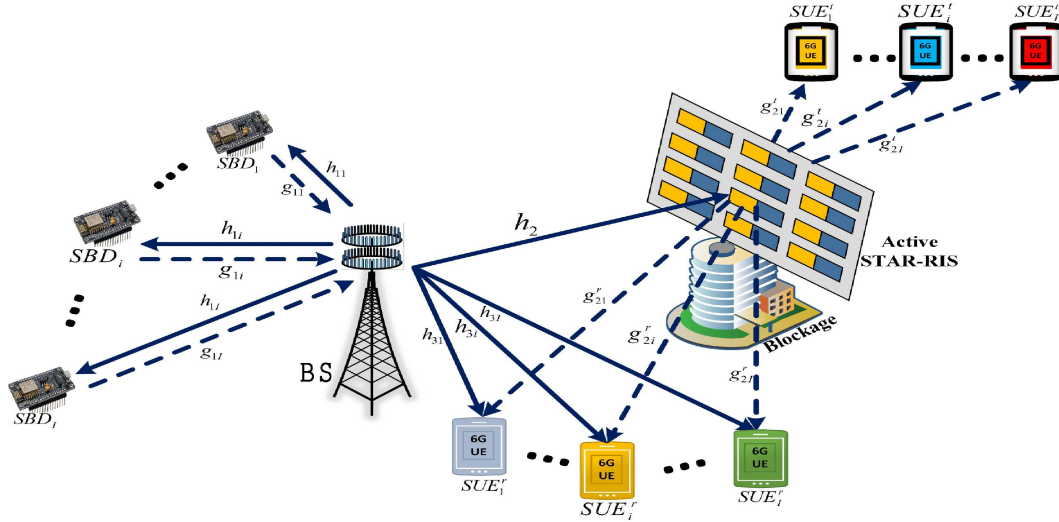


Fig. 1: Symbiotic radio system model with SBDs, STAR-RIS and SUEs

transmit beamforming vector $\mathbf{w}_{1i} \in \mathbb{C}^{N \times 1}$ and with power P_i . The received signal at SBD_i can be obtained as follows:

$$y_k^{SBD_i}(t) = \sqrt{P_i} \mathbf{h}_{1i}^H \mathbf{w}_{1i} s_k(t) + n_k^{SBD_i}(t), \forall i \in \psi \quad (3)$$

where $\psi \triangleq \{1, 2, \dots, i, \dots, I\}$ represents the collection of all SBDs and all SUEs.

In this paper, we use NOMA to enable multiple access for users, optimize resource allocation among them, and prevent excessive interference at the destination. Therefore, the BS transmits signals to each of the SBDs with different power levels based on their distances and channels gain. As shown in Fig. 1, the allocated power to the SBDs is in the form of $P_I > \dots > P_i > \dots > P_1$. Here, we assume that the transmitted symbol from the ambient signal sent to all SBDs is the same and equal to $s_k(t)$.

Upon receiving the ambient signal $y_k^{SBD_i}(t)$, the SBDs harvests energy for its electronic circuits and subsequently modulates its information, denoted as $c_i(t)$, $i \in \psi$, onto the carrier signal. It then backscatters the modulated signal back to the BS using the SBD's reflection coefficient η_i , $0 \leq \eta_i \leq 1$. It should be noted that since SBD does not have any power-consuming active components, $n_k^{SBD_i}(t)$, which is the complex gaussian noise at the SBD's antenna, can be disregarded. Assuming that the beamforming vector used during signal reception at the BS is denoted as $\mathbf{w}_{Ri}^H \in \mathbb{C}^{1 \times N}$, we can express the received signal at the BS as follows.

$$y_k^{BS}(t) = s_k(t) \sum_{j \in \psi} \sqrt{P_j} \eta_j \mathbf{w}_{Rj}^H \mathbf{g}_{1j} \mathbf{h}_{1j}^H \mathbf{w}_{1j} c_j(t) + n_k^{BS}(t) \quad (4)$$

where $n_k^{BS} \sim \mathcal{CN}(0, \sigma_{BS}^2)$ is the circularly symmetric complex gaussian (CSCG) noise at the BS and $\mathbf{g}_{1i} \in \mathbb{C}^{N \times 1}$ is the complex channel vector from SBD_i to BS.

In this paper, we assume that all channels experience are flat fading and remain constant within a given time frames. It is important to note that the channel state information (CSI) for all channels is readily available.

The BS is designed with a robust infrastructure and powerful processors, which enable it to perform complex signal processing tasks. Moreover, since the signal $s_k(t)$ is specific to the BS and well-known, and given the availability of CSI for channels \mathbf{g}_{1i} and \mathbf{h}_{1i}^H , the BS is capable of efficiently extracting the information $c_i(t)$ for SBD_i in its baseband and remove any other noise from it. Furthermore, to eliminate interference caused by other SBDs, which have a stronger Signal-to-Interference-plus-Noise Ratio (SINR) compared to SBD_i and simultaneously transmit their signals to the base station, the successive interference cancellation (SIC) method is employed.

So far, the desired signal for SBD_i has been received and decode by the BS. To enhance the reception quality, the BS receiver employs Maximal-Ratio Combining (MRC) technique. The receiving beamforming vector, denoted as $\mathbf{w}_{Ri} = \mathbf{g}_{1i}/\|\mathbf{g}_{1i}\|$, is utilized for this purpose. Considering Eq. 4 and taking into account $\mathbb{E}[|s_k(t)|^2] = 1$, the maximum achievable rate, denoted as R_{1-SBD_i} , after implementing the SIC technique at the BS during the first phase can be determined as follows:

$$R_{1-SBD_i} = \frac{B\tau_i}{K} \log_2 \left(1 + \frac{K P_i \eta_i \|\mathbf{g}_{1i}\|^2 |\mathbf{h}_{1i}^H \mathbf{w}_{1i}|^2}{\sum_{j \in v} P_j \eta_j \|\mathbf{g}_{1j}\|^2 |\mathbf{h}_{1j}^H \mathbf{w}_{1j}|^2 + B \sigma_{BS}^2} \right) \quad (5)$$

where B represents the bandwidth of the receiver filter in the BS, $v \triangleq \{1, \dots, i-1\}$ represents the set of all SBDs whose distance to BS is less than SBD_i and as a result have higher channel gain. These SBDs cause interference on SBD_i , whose total interference is shown in the denominator of the SINR fraction. Also, τ_i denotes the allocated time for completing the first phase.

In the second phase, the BS transmits the signal $c_i(t)$, $i \in \psi$ to the destinations ASRIS and SUE_i , $i \in \psi$. Specifically, SUE_i is located in the reflection space of ASRIS, denoted as SUE_i^r . Both ASRIS and SUE_i have direct links with the BS. The transmission is carried out with a power P_i to SUE_i using the beamforming vector $\mathbf{w}_{2i} \in \mathbb{C}^{N \times 1}$. In this section, we also utilize NOMA for accessing multiple SUEs present in the reflecting space of ASRIS. In this scenario, SUEs are located at different distances from BS and ASRIS, and therefore, the power of the

transmitted signal is allocated based on their distance and channels gain. In this scenario, the received signal that reaches the ASRIS through the channel $\mathbf{h}_2^H \in \mathbb{C}^{M \times N}$ can be expressed as follows

$$\mathbf{y}_{ASRIS}(t) = \mathbf{h}_2^H \sum_{j \in \psi} \sqrt{P_j} \mathbf{w}_{2j} c_j(t) + \mathbf{n}_{ASRIS}(t) \quad (6)$$

As mentioned above, since the ASRIS has active components, the presence of CSCG noise, denoted as $\mathbf{n}_{ASRIS} \sim \mathcal{CN}(\mathbf{0}, \sigma_{ASRIS}^2 \mathbf{I}_M)$, should be taken into account.

On the other hand, considering Fig. 1, the received signal at SUE_i^r , which arrives through both the direct link from the BS and the reflected signal from ASRIS, can be obtained as follows.

$$y_{SUE_i}^r(t) = \sum_{j \in \psi} \sqrt{P_j} (\mathbf{g}_{2j}^r \Theta_r \mathbf{h}_2^H + \mathbf{h}_{3j}^H) \mathbf{w}_{2j} c_j(t) + \left(\sum_{j \in \psi} \mathbf{g}_{2j}^r \right) \Theta_r \mathbf{n}_{ASRIS}(t) + n_{SUE_i}^r(t) \quad (7)$$

where $\mathbf{g}_{2i}^r \in \mathbb{C}^{1 \times M}$ is the channel vector between BS and SUE_i^r in the reflection space of the ASRIS, $\mathbf{h}_{3i}^H \in \mathbb{C}^{1 \times N}$ is the channel vector for the direct link between BS and SUE_i^r , and $n_{SUE_i}^r \sim \mathcal{CN}(0, \sigma_{SUE_i}^2)$ is the CSCG noise at the SUE_i^r .

according to the Eq. 7 the maximum achievable rate after using the SIC technique in the SUE_i^r , denoted as $R_{2-SUE_i}^r$, in the second phase for the SUE_i^r . is:

$$R_{2-SUE_i}^r = B(1 - \tau_i) \log_2 \left(1 + \frac{P_i \mathbf{w}_{2i}^2 |\mathbf{g}_{2i}^r \Theta_r \mathbf{h}_2^H + \mathbf{h}_{3i}^H|^2}{\sum_{j \in \psi} P_j \mathbf{w}_{2j}^2 |\mathbf{g}_{2j}^r \Theta_r \mathbf{h}_2^H + \mathbf{h}_{3j}^H|^2 + B \left(\left\| \Theta_r \sum_{j \in \psi} \mathbf{g}_{2j}^r \right\|^2 \sigma_{ASRIS}^2 + \sigma_{SUE_i}^2 \right)} \right) \quad (8)$$

where $1 - \tau_i$ denotes the allocated time for completing the second phase. In this relation, v represents the set of all SUEs in reflection space, whose channels gain (BS- SUE^r and BS-ASRIS- SUE^r) is higher than SUE_i^r and as a result have lower power allocation.

Also, due to blockage, a direct link between the BS and SUE_i in the transmission space (SUE_i^t) of ASRIS is not available. Consequently, only ASRIS has the capability to transmit the signal to SUE_i^t using its own transmission space. It's important to note that if any other structure, such as an active or passive RIS, were used instead of ASRIS, SUE_i^t would be located in a cellular blind spot. In this scenario, the received signal at SUE_i^t , which arrives through the transmission link by ASRIS, can be obtained as follows:

$$y_{SUE_i}^t(t) = \sum_{j \in \psi} \sqrt{P_j} (\mathbf{g}_{2j}^t \Theta_t \mathbf{h}_2^H) \mathbf{w}_{2j} c_j(t) + \left(\sum_{j \in \psi} \mathbf{g}_{2j}^t \right) \Theta_t \mathbf{n}_{ASRIS}(t) + n_{SUE_i}^t(t) \quad (9)$$

where $\mathbf{g}_{2i}^t \in \mathbb{C}^{1 \times M}$ is the channel vector between BS and SUE_i^t in the transmission space of the ASRIS, and $n_{SUE_i}^t \sim CN(0, \sigma_{SUE_i}^2)$ is the CSCG noise at the SUE_i^t .

according to the Eq. 9 the maximum achievable rate after using the SIC technique in the SUE_i^t , denoted as $R_{2-SUE_i}^t$, in the second phase for the SUE_i^t is:

$$R_{2-SUE_i}^t = B(1 - \tau_i) \log_2 \left(1 + \frac{P_i |\mathbf{g}_{2i}^t \mathbf{\Theta}_t \mathbf{h}_2^H \mathbf{w}_{2i}|^2}{\sum_{j \in v} P_j \mathbf{w}_{2j}^2 |\mathbf{g}_{2j}^t \mathbf{\Theta}_t \mathbf{h}_2^H|^2 + B \left(\left\| \mathbf{\Theta}_t \sum_{j \in \psi} \mathbf{g}_{2j}^t \right\|^2 \sigma_{ASRIS}^2 + \sigma_{SUE_i}^2 \right)} \right) \quad (10)$$

where $v \triangleq \{1, \dots, i-1\}$ represents the set of all SUEs whose distance to ASRIS is less than SUE_i^t and as a result have higher channel gain. Without loss of generality, for the sake of simplicity, we can consider the bandwidth is $B = 1Hz$.

It should be noted that in this article, all communication channels with ASRIS are considered to be rician, and all communication channels with BS are considered to be rayleigh. Additionally, due to the direct line of sight between BS and ASRIS, we also consider this channel to be rician.

III. SUM THROUGHPUT MAXIMIZATION

Based on the explanations provided in the preceding section and in accordance with equations 5, 8, and 10, the main objective of this article is to maximize the sum throughput. For this purpose, we define the optimization problem as follows:

$$\underset{\eta_i, \mathbf{\Theta}_t, \tau_i, P_i}{Max} \min (R_{1-SBD_i}, R_{2-SUE_i}^l) \quad (11a)$$

S.t

$$|s_m|^2 = |t_m|^2 + |r_m|^2, \quad \forall m \in \mathcal{M}, \text{ (only for Passive SRIS)} \quad (11b)$$

$$(|\beta_m^t|^2, |\beta_m^r|^2) \leq \frac{p_{ASRIS}}{2}, \quad p_{ASRIS} = \text{cte}, \text{ (only for ASRIS)} \quad (11c)$$

$$0 \leq \theta_m^l \leq 2\pi, \quad \forall m \in \mathcal{M} \quad (11d)$$

$$p_i \leq p_{BS}, \quad i \in \psi, p_{BS} = \text{cte} \quad (11e)$$

$$0 \leq \eta_i \leq 1, 0 \leq \tau_i \leq 1, \quad i \in \psi \quad (11f)$$

$$\varepsilon_{SBD_i} \leq \Gamma P_i (1 - \eta_i) (1 - \tau_i) |\mathbf{h}_{1i}^H \mathbf{w}_{1i}|^2, \quad i \in \psi \quad (11g)$$

$$R_{1-SBD_i} > R_{1-SBD_{i+1}}, \quad i \in \psi \quad (11h)$$

$$R_{2-SUE_i}^l > R_{2-SUE_{i+1}}^l, \quad i \in \psi \quad (11i)$$

where, $0 \leq \Gamma \leq 1$ is the energy conversion efficiency by SBDs and (11g) restricts the energy harvested by the SBD_i to its maximum specified value. Also, to guarantee the SIC performed successfully in two phases, the conditions (11h) and (11i) should be satisfied.

To make the optimization problem (11) implementable, certain modifications are required. Given the requirement of uninterrupted and collision-free transmission of information from SBD_i to the SUE_i^r or SUE_i^t , the maximum achievable throughput is attained when $R_{1-SBD_i} = R_{2-SUE_i}^r = R_{2-SUE_i}^t = R$. Therefore, the final optimization problem for maximizing the achievable rate can be stated as follows:

$$\underset{R, \eta_i, \mathbf{w}_{1i}, \mathbf{w}_{2i}, \tau_i, P_i, \beta_m^l, \theta_m^l}{Max} R \quad (12a)$$

S.t

$$2^{\left(\frac{KR}{\tau_i}\right)} - 1 \leq \frac{K P_i \eta_i \|\mathbf{g}_{1i}\|^2 |\mathbf{h}_{1i}^H \mathbf{w}_{1i}|^2}{\sum_{j \in \psi} P_j \eta_j \|\mathbf{g}_{1j}\|^2 |\mathbf{h}_{1j}^H \mathbf{w}_{1j}|^2 + \sigma_{BS}^2} \quad (12b)$$

$$2^{\left(\frac{R}{1-\tau_i}\right)} - 1 \leq \frac{P_i \mathbf{w}_{2i}^2 |\mathbf{g}_{2i}^r \Theta_r \mathbf{h}_2^H + \mathbf{h}_{3i}^H|^2}{\sum_{j \in \psi} P_j \mathbf{w}_{2j}^2 |\mathbf{g}_{2j}^r \Theta_r \mathbf{h}_2^H + \mathbf{h}_{3j}^H|^2 + \left(\left\| \Theta_r \sum_{j \in \psi} \mathbf{g}_{2j}^r \right\|^2 \sigma_{ASRIS}^2 + \sigma_{SUE_i}^2 \right)}, \text{ (when } l = r) \quad (12c)$$

$$2^{\left(\frac{R}{1-\tau_i}\right)} - 1 \leq \frac{P_i |\mathbf{g}_{2i}^t \Theta_t \mathbf{h}_2^H \mathbf{w}_{2i}|^2}{\sum_{j \in \psi} P_j \mathbf{w}_{2j}^2 |\mathbf{g}_{2j}^t \Theta_t \mathbf{h}_2^H|^2 + \left(\left\| \Theta_t \sum_{j \in \psi} \mathbf{g}_{2j}^t \right\|^2 \sigma_{ASRIS}^2 + \sigma_{SUE_i}^2 \right)}, \text{ (when } l = t) \quad (12d)$$

$$(11b), (11c), (11d), (11e), (11f), (11g), (11h), (11i) \quad (12e)$$

The Eq.12 is a non-convex problem that can be implemented with the algorithms based of deep reinforcement learning (DRL).

IV. DEEP REINFORCEMENT LEARNING

In this section, we initially transform the non-convex problem 12 into a model-free Markov decision process (MDP). Subsequently, we develop DRL algorithms utilizing PPO, TD3 and A3C to address and resolve problem 12.

A. MDP

The MDP formulation constructs a 4-tuple, denoted as $(\mathbf{s}_t, \mathbf{a}_t, \mathbf{r}_t, \mathbf{s}_{t+1})$, where the current state, action, reward function, and next state are represented by \mathbf{s}_t , \mathbf{a}_t , r_t , and \mathbf{s}_{t+1} , respectively. The agent interacts with the environment, observing the current state \mathbf{s}_t from the state space \mathcal{S} with \mathbf{s}_t and selecting action \mathbf{a}_t from the action space \mathcal{A} with \mathbf{a}_t according to its policy. Additionally, the formulation of problem 12 further details the state, action, and reward function.

1) *State*: The current state $\mathbf{s}_t \in \mathcal{S}$ at time step t encompasses crucial environmental information associated with problem 12. This configuration enables the policy to improve and adjust in response to the dynamic environment. To elaborate, the state \mathbf{s}_t for the analyzed system includes the all channels of environment expressed as follows:

$$\mathbf{s}_t = \{h_{1i}, h_2, h_{3i}, g_{1i}, g_{2i}^l\}, \quad \forall i \in \psi, \forall t \in T, l = r, t \quad (13)$$

2) *Action*: The term action denoted by $\mathbf{a}_t \in \mathcal{A}$ at time step t encompasses the decisions and choices undertaken by an agent as it interacts with the relevant states. These actions represent the agent's responses and strategies employed to navigate and influence the dynamics of the considered system during the specified time instance [36]. Every variable within problem 12 serves as an action, implying that each element or parameter in the problem formulation represents a distinct decision or manoeuvre in addressing and resolving the challenges posed by the problem. In essence, these variables act as the modifiable components through which the agent, system, or solver can influence and effect changes in pursuit of optimal solutions or outcomes for problem 12. As a result, the set of actions can be described as follows:

$$\mathbf{a}_t = \{R, \eta_i, \mathbf{w}_{1i}, \mathbf{w}_{2i}, \tau_i, P_i, \beta_m^l, \theta_m^l\}, \quad \forall i \in \psi, \forall m \in \mathcal{M}, \forall t \in T, l = r, t \quad (14)$$

3) *Reward*: The DRL methodologies instruct agents to make appropriate decisions to maximize the reward. In the optimization problem 12, the reward function aligns with the objective function, guiding the training process towards actions that contribute to the overall goal of optimizing the specified objective.

$$\mathbf{r}_t = R_t + \sum_{j=1}^{11} l_{C_j}, \quad \forall t \in T \quad (15)$$

where $l_{C_j} = \alpha_j R$, and the index j corresponds to all constraints, i.e., $\forall j \in \{1, 2, \dots, 11\}$. Besides, $\alpha_j = 1$, if the C_j -th constraint is satisfied and $\alpha_j = 0$, otherwise.

B. PPO Algorithm

The PPO algorithm, functioning as an actor-critic on-policy gradient method, simplifies the intricate computations involved in earlier policy gradient methods like trust region policy optimization (TRPO) [37].

In the context of reinforcement learning, the main objective is to maximize the expected cumulative reward, taking into account a protracted temporal process. Consequently, the cumulative reward at time step t is represented as $\mathcal{R}_t = \sum_{t=0}^{\infty} \lambda^t r_t$, where $\lambda \in [0, 1)$ signifies the discount factor. To delve into specifics, both actor and critic networks are employed to portray the parameterized stochastic policy of action selection, denoted as $\pi_{\theta}(\mathbf{a}_t|\mathbf{s}_t)$, and the state-value function $V_{\phi}(\mathbf{s}_t)$, respectively. Here, θ and ϕ stand for the parameters of the actor and critic networks. Subsequently, a surrogate objective function, constructed based on the PPO approach, can be articulated as follows:

$$\mathcal{L}(\theta, \mathbf{s}_t, \mathbf{a}_t) = \mathbb{E}[\beta_t(\theta)\Omega(\mathbf{s}_t, \mathbf{a}_t)]. \quad (16)$$

The probability ratio between the current policy and the previous one is denoted as $\beta_t(\theta) = \pi_{\theta}(\mathbf{a}_t|\mathbf{s}_t)/\pi_{\theta^{\text{old}}}(\mathbf{a}_t|\mathbf{s}_t)$, where θ^{old} represents the parameter associated with the old policy in the actor network. Additionally, the advantage function is expressed as follows:

$$\Omega(\mathbf{s}_t, \mathbf{a}_t) = r(\mathbf{s}_t, \mathbf{a}_t) + \lambda V_{\phi^{\text{old}}}(\mathbf{s}_{t+1}) - V_{\phi^{\text{old}}}(\mathbf{s}_t), \quad (17)$$

where ϕ^{old} signifies the parameter associated with the critic network for the previous state-value estimation function. Subsequently, a mini-batch stochastic gradient descent (SGD) technique is employed to update the associated θ across a set of Q transitions denoted as $(\mathbf{s}_t^q, \mathbf{a}_t^q, \mathbf{r}_t^q, \mathbf{s}_{t+1}^q)$ sampled from an experience buffer, which is given by:

$$\theta = \theta^{\text{old}} - \delta_A \frac{1}{Q} \sum_{q=1}^Q \nabla_{\theta} \tilde{\mathcal{L}}_q(\theta, \mathbf{s}_t^q, \mathbf{a}_t^q), \quad (18)$$

Where δ_A denotes the learning rate, and $\tilde{\mathcal{L}}_q(\theta, \mathbf{s}_t^q, \mathbf{a}_t^q)$ represents the instantiation of $\mathcal{L}(\theta, \mathbf{s}_t, \mathbf{a}_t)$ with the q -th transition, respectively. The mini-batch stochastic gradient descent (SGD) utilized for updating ϕ employs the mean squared error (MSE) loss function in the following manner:

$$\phi = \phi^{\text{old}} - \delta_C \frac{1}{Q} \sum_{q=1}^Q \nabla_{\phi} (V_{\phi}(\mathbf{s}_t^q) - \hat{\mathcal{R}}(\mathbf{s}_t^q, \mathbf{a}_t^q))^2, \quad (19)$$

where the learning rate is denoted as δ_C . Additionally, the target state-value function, indicated as $\hat{R}(\mathbf{s}_t, \mathbf{a}_t)$, is expressed as:

$$\hat{R}(\mathbf{s}_t, \mathbf{a}_t) = r(\mathbf{s}_t, \mathbf{a}_t) + \lambda V_{\phi^{\text{old}}}(\mathbf{s}_{t+1}). \quad (20)$$

The PPO-based approach are outlined in Algorithm (1). To elaborate, the action \mathbf{a}_t is generated based on the particular policy within the current state \mathbf{s}_t , resulting in the acquisition of the reward \mathbf{r}_t . Subsequently, the transition $(\mathbf{s}_t, \mathbf{a}_t, \mathbf{r}_t, \mathbf{s}_{t+1})$ is recorded in the experience buffer, from which Q instances are sampled. In the following, the advantage function $\Omega(\mathbf{s}_t, \mathbf{a}_t)$ in (17) is computed. Finally, the relevant actor and critic parameters undergo updating through mini-batch SGD.

Algorithm 1 The PPO Algorithm

- 1- Initialize the environment parameters as well as the parameters of actor and critic networks, i.e., $\theta, \phi, \varepsilon, \delta_A$ and δ_C
 - 2- Set $\theta^{\text{old}} = \theta$ and $\phi^{\text{old}} = \phi$
 - 3- **For** each episode do
 - 4- Reset environment and initialize position of users randomly
 - 5- Initialize state \mathbf{s}_0 according to 13
 - 6- **For** each step do
 - 7- Generate action \mathbf{a}_t according to $\pi_{\theta}(\mathbf{a}_t|\mathbf{s}_t)$ in state \mathbf{s}_t
 - 8- Calculate reward \mathbf{r}_t
 - 9- Observe the new state \mathbf{s}_{t+1}
 - 10- Store $(\mathbf{s}_t, \mathbf{a}_t, \mathbf{r}_t, \mathbf{s}_{t+1})$ in the experience buffer
 - 11- Calculate the advantage function $\Omega(\mathbf{s}_t, \mathbf{a}_t)$ in (17)
 - 12- Calculate $\nabla_{\theta} \tilde{\mathcal{L}}_q(\theta, \mathbf{s}_t^q, \mathbf{a}_t^q)$ in (18)
 - 13- Calculate $\nabla_{\phi} (V_{\phi}(\mathbf{s}_t^q) - \hat{R}(\mathbf{s}_t^q, \mathbf{a}_t^q))^2$ in (19)
 - 14- Calculate $\hat{R}(\mathbf{s}_t, \mathbf{a}_t)$ in (20)
 - 15- Update θ and ϕ in (18) and (19), respectively
 - 16- Update $\theta^{\text{old}} = \theta$ and $\phi^{\text{old}} = \phi$
 - 17- **End FOR**
 - 18- **End FOR**
-

C. TD3 Algorithm

The TD3 algorithm represents a reinforcement learning approach that is both model-free and off-policy. The state-action value function as follows:

$$q_\mu(\mathbf{s}_t, \mathbf{a}_t) = \mathbb{E}_{\Pr(\mathbf{s}_{t+1}|\mathbf{s}_t, \mathbf{a}_t)} \left[\sum_{t=0}^{\infty} \gamma^t r(\mathbf{s}_t, \mu(\mathbf{s}_t) | \mathbf{s}_t = \mathbf{s}_0, \mathbf{a}_t = \mu(\mathbf{s}_0)) \right], \quad (21)$$

where μ is parameters of the actor network, and $\gamma \in (0, 1]$ denotes the discount factor. The optimal policy is given by

$$\mu^*(\mathbf{s}_t) = \arg \max_{\mu(\mathbf{s}_t) \in \mathcal{A}} q_\mu(\mathbf{s}_t, \mu(\mathbf{s}_t)). \quad (22)$$

TD3 represents an enhanced iteration of the deep deterministic policy gradient (DDPG), introducing adjustments to mitigate the overestimation of state-action value and avert the generation of sub-optimal policies [38]. The specifics of these modifications are elaborated in the training network description. Similar to the PPO algorithm, the agent chooses its action based on the observed state, and the corresponding experience $(\mathbf{s}_t, \mathbf{a}_t, \mathbf{r}_t, \mathbf{s}_{t+1})$ is stored in the buffer. Consequently, the loss function for critic networks with parameter α_i is calculated as follows.

$$\mathcal{L}(\alpha_i) = \frac{1}{|B|} \sum_{k=1}^B \left(q_\mu(\mathbf{s}_t^k, \mathbf{a}_t^k; \alpha_i) - y(r_t^k, \mathbf{s}_{t+1}^k) \right)^2, \quad (23)$$

where y is calculated by

$$y(r_t^k, \mathbf{s}_{t+1}^k) = r_t^k + \gamma \min_i q_{\mu_i}(\mathbf{s}_{t+1}^k, \tilde{\mathbf{a}}_{t+1}^k; \bar{\alpha}_i). \quad (24)$$

To adjust the parameters of critic networks, α_i , the gradient descent algorithm is employed on the loss function (23) using the following equation:

$$\alpha_i = \alpha_i - \theta_i \nabla_{\alpha_i} \mathcal{L}(\alpha_i), \quad (25)$$

where θ_i represents the learning rate. Also, the loss function and update parameters of the actor network are as follows:

$$\mathcal{L}(\mu) = \frac{1}{|B|} \sum_{k=1}^B q_\mu(\mathbf{s}_t^k, \mathbf{a}_t^k). \quad (26)$$

$$\mu = \mu - \tilde{\theta} \nabla_{\mu} \mathcal{L}(\mu). \quad (27)$$

The pseudo-code for the TD3 algorithm is presented in Algorithm 2.

Algorithm 2 The TD3 Algorithm

- 1- Initialize the environment and networks parameters, i.e., α , and μ
 - 2- Set $\theta^{\text{old}} = \theta$ and $\phi^{\text{old}} = \phi$
 - 3- **For** each episode do
 - 4- Reset environment and initialize position of users randomly
 - 5- Initialize state \mathbf{s}_0 according to 13
 - 6- **For** each step do
 - 7- Observe state \mathbf{s}_t and select action \mathbf{a}_t
 - 8- Observe next state \mathbf{s}_{t+1} and receive reward r_t
 - 9- Store $(\mathbf{s}_t, \mathbf{a}_t, r_t, \mathbf{s}_{t+1})$ in \mathcal{M} .
 - 10- Randomly sample a batch set B from replay buffer
 - 11- Update the network parameters α_i , and μ using (25), (27), respectively.
 - 12- **End FOR**
 - 13- **End FOR**
-

D. A3C algorithm

The A3C algorithm employs an actor-critic architecture, where an actor network makes policy decisions and a critic network evaluates the value of these decisions. The "Advantage" in A3C refers to the use of an advantage function, which measures the advantage of taking a particular action in a given state over the average action value [39]. the advantage function is used to decrease the variance in estimation, as expressed by the following equation:

$$\mathcal{A}_t(\mathbf{s}_t, \mathbf{r}_t; \mu, \alpha) = \mathcal{R}_t - V(\mathbf{s}_t; \alpha), \quad (28)$$

where μ and α are the parameters of actor and critic network, respectively. Furthermore, \mathcal{R} represents cumulative reward as follows:

$$\mathcal{R} = \sum_{i=0}^k \gamma^i r_{t+i} + \gamma^k V(\mathbf{s}_{t+k}; \alpha), \quad (29)$$

where k is the number of steps which A3C used for parameter updating.

Derived from the advantage function \mathcal{A}_t the actor's loss function is expressed as:

$$f_{\pi}(\mu) = \log \pi(a_t | \mathbf{s}_t; \mu) (\mathcal{A}_t) + \beta H(\pi(\mathbf{s}_t; \mu)), \quad (30)$$

Here, $H(\pi(\mathbf{s}_t; \mu))$ represents an entropy term incorporated to promote exploration during training, preventing potential premature convergence [40]. The parameter β is utilized to regulate the

intensity of entropy regularization, facilitating the balance between exploration and exploitation. The loss function for the estimated critic network is specified as:

$$f(\alpha) = (\mathcal{R}_t - V(s_t; \alpha))^2. \quad (31)$$

This is employed to update the value function $V(st; \theta_v)$. The update for the critic is executed using the following accumulated gradient.

$$d\alpha \leftarrow d\alpha + \frac{\partial(\mathcal{R}_t - V(s_t; \alpha))^2}{\partial\alpha}. \quad (32)$$

The actor undergoes an update through the following process:

$$d\mu \leftarrow d\mu + \nabla_{\mu'} \log \pi(a_t | s_t; \mu') (\mathcal{A}_t) + \beta \nabla_{\mu'} H(\pi(s_t; \mu')). \quad (33)$$

All the steps of the A3C algorithm are outlined in Algorithm 3.

Algorithm 3 The A3C Algorithm

- 1- Initialize the global actor network and global critic network with parameters, α , and μ
 - 2- Initialize the thread-specific actor and thread-specific critic network parameters α' , and μ'
 - 3- **For** each episode do
 - 4- Reset environment and initialize position of users randomly
 - 5- **For** each worker do
 - 6- Initialize the gradients of global agent: $d\alpha = 0$, $d\mu = 0$
 - 7- Synchronous parameters of each worker with global parameters $\alpha' = \alpha$, and $\mu' = \mu$
 - 6- Obtain initial state s_0 .
 - 7- **For** each step do
 - 8- Perform at under policy $\pi(s_t; \mu')$
 - 9- Obtain reward r_t and new state s_{t+1}
 - 10- **End FOR**
 - 11- $R = \begin{cases} 0, & \text{for terminal state} \\ V(s_t; \alpha'), & \text{for non-terminal state} \end{cases}$
 - 12- $R = r_t + \gamma R$
 - 13- Obtain accumulate gradient α based on (32)
 - 14- Obtain accumulate gradient μ based on (33)
 - 15- **End FOR**
 - 16- **End FOR**
-

In the following, each of the PPO, TD3, and A3C methods, modeling and simulations are conducted, and the outputs of each are compared with each other in relation to this modeling system.

TABLE I: Parameters set in the learning simulation.

Parameters	PPO	TD3	A3C
Number/Size of Actor, Critic	2/128,128	2/400,300	2/128,128
Min Batch Size	32	64	64
Critic/Actor Learning Rate	0.001/0.0001	0.001/0.0001	0.001/0.0001
Target Network Update	0.0005	0.0005	0.0005
Discount Factor	0.99	0.99	0.99
Policy Entropy Coefficient	0.01	-	-
Number of Workers	-	-	3
Number of Episodes	30000	30000	30000
Number of Steps	200	200	200

V. SIMULATION RESULTS

According to the proposed model, SBDs and SUEs are randomly distributed across the network space, as depicted in Fig. 1. In all simulations, constant values of $K = 100$, Rician factor = 10, and $\sigma_{ASRIS}^2 = \sigma_{BS}^2 = \sigma_{SUE}^2 = -120$ dBm have been considered. Additionally, we assume the carrier frequency of the ambient signal is 28 GHz, the path loss exponent is 3, and the antenna gain of the BS and ASRIS is 16 and 8 watt, respectively. All simulation results are generated by averaging over 100 random channels. The distance between the BS and SBD is 200 meters, and the maximum distance of BSs from SUEs and ASRIS is 100 and 300 meters, respectively.

The simulations were carried out on a laptop featuring an Intel Core i7-6500U 8 GB DDR3-RAM. It should be noted that the parameters related to learning simulation for each method are given in Table I.

A. Convergence of the Proposed Methods

As described, in this paper, we utilized three learning methods, namely PPO, TD3, and A3C, to tackle the non convex optimization problem. In this scenario, the convergence plot for each of these methods is depicted in Fig. 2.

Based on the information presented in Fig. 2, it is clear that the A3C method exhibits markedly superior convergence compared to the other two methods. Specifically, the convergence points for PPO, TD3, and A3C occur at approximately 17000, 22000, and 5000 episodes, respectively. These values signify the completion of network learning for each method.

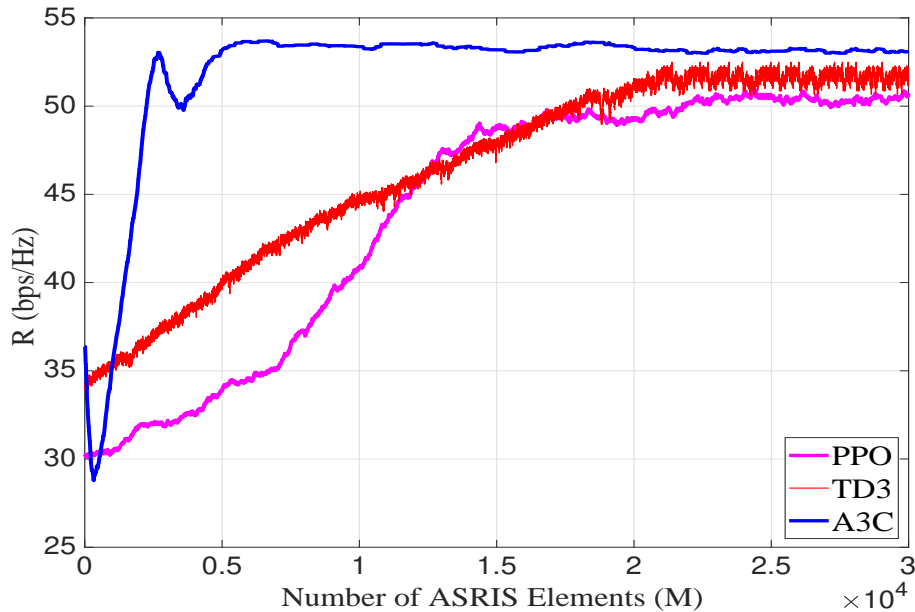


Fig. 2: Convergence plot of the three learning methods, PPO, TD3, and A3C, in the case of $N = 8, M = 16, I = 3, \varepsilon_{SBD_i} = 1\mu W$.

B. Sum Throughput Maximization Based on Energy Harvesting by SBDs

In the design of passive symbiotic radio networks, a pivotal factor is the quantity of energy harvested by the SBD devices. In this section, adhering to the constraint outlined in Eq. 11g, we depict the rate of information exchange in the network as it correlates with the fluctuations in the energy harvesting capacity for each SBD.

As illustrated in Fig. 3, it is evident that as the energy harvesting capability of the devices increases, indicating a higher capacity to store energy from ambient waves, the information throughput in the network also rises. It is worth noting that the average energy required for transmitting a pulse by passive IoT devices is about 1-10 μW [41]–[44].

Moreover, in this approach, it is apparent that utilizing the A3C algorithm leads to an increase in the total information exchange rate compared to the other two methods.

C. Sum Throughput Maximization Versus Transmit Power of BS and ASRIS

Since both BS and STAR-RIS are considered active in the proposed system model, in this section, we investigate the impact of the transmit power of each on the network's performance.

In Figure 4, we investigate the influence of augmenting the transmit power of the BS from 4 to 32 watts across all three methods. Additionally, Figure 5 illustrates the consequences of

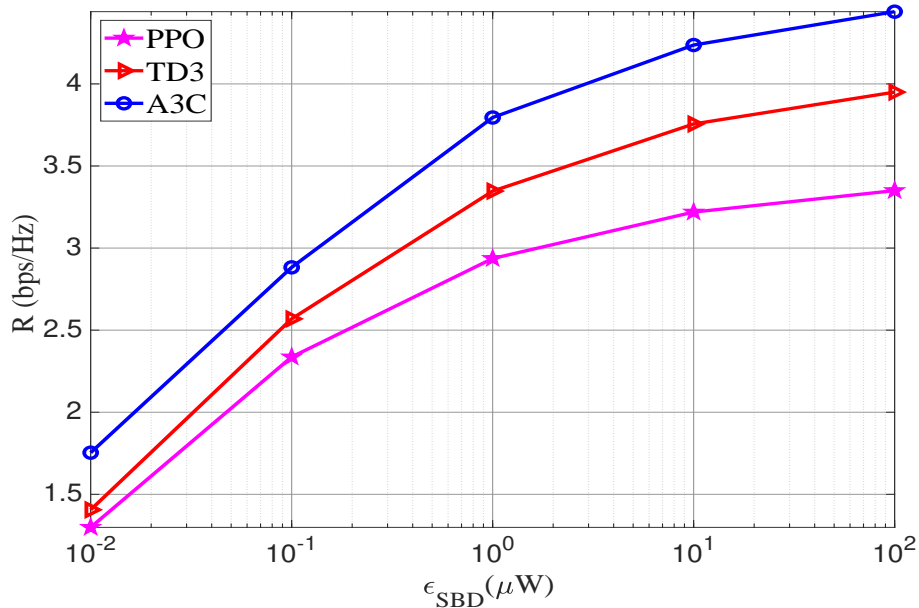


Fig. 3: Sum throughput maximization based on the energy harvested by SBDs in all three methods, PPO, TD3, and A3C, under the conditions $N = 8, M = 16, I = 3$.

amplifying the transmit power of the ASRIS from 2 to 16 watts, which is caused by the reflection and transmission of the signals by it. The analysis encompasses all three methods, namely PPO, TD3, and A3C.

As expected, with the increase in the transmit power of signals in each BS or ASRIS, the data rate also increases. According to Figs. 5 and 4, the A3C, TD3, and PPO methods allocate the highest processing efficiency for optimal resource allocation among users, consequently increasing the users' information rate. Also, considering the convergence depicted in Fig. 2, indicating better convergence of the A3C method compared to the other two methods, we conclude that this method is more suitable for modeling and implementing the proposed system in this research.

D. Sum Throughput Maximization Versus the Number of Elements in BS and ASRIS

As mentioned in the first part of this chapter, our system model incorporates a BS equipped with Massive MIMO antennas and an active STAR-RIS within the network. In this section, our objective is to examine the influence on the sum data rate of all users in the network by manipulating the number of elements in both the BS and ASRIS. To begin, we illustrate this chart for the PPO method as follows.

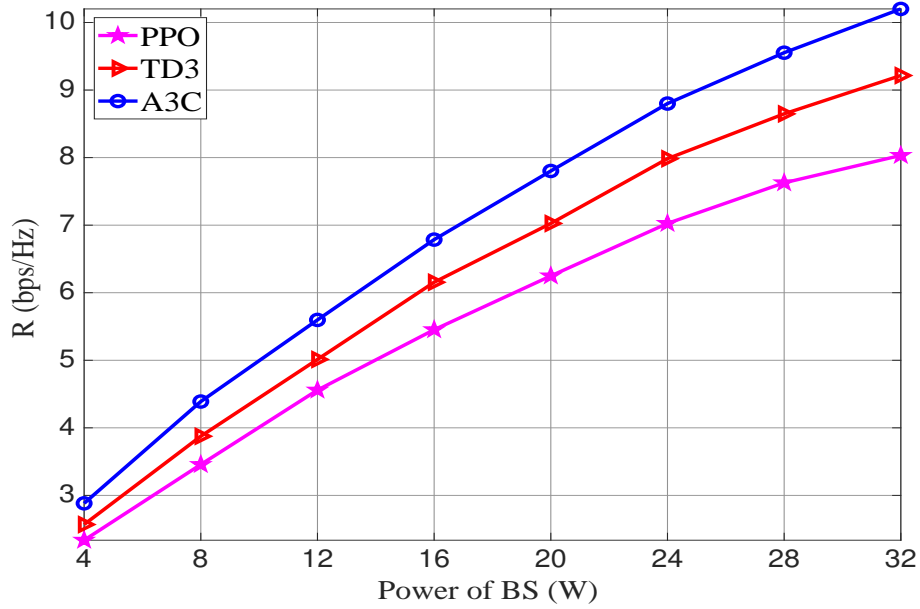


Fig. 4: Impact of increasing the transmitted signal power at the BS in relation to the sum user data rate in the case of $N = 8, M = 16, I = 3, \varepsilon_{SBD_i} = 1\mu W, P_{ASRIS} = 10W$.

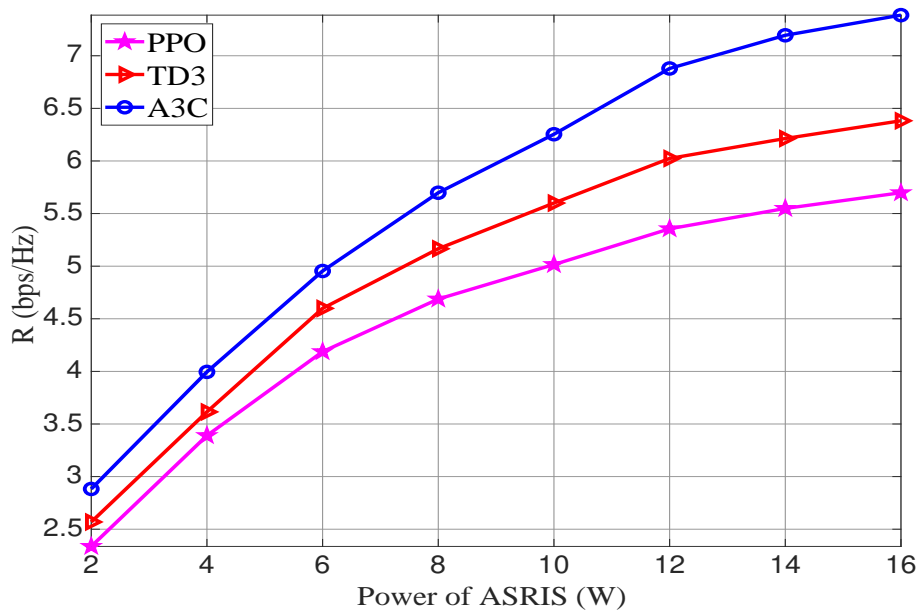


Fig. 5: Impact of increasing the transmitted signal power in ASRIS in relation to the sum user data rate in the case of $N = 8, M = 16, I = 3, \varepsilon_{SBD_i} = 1\mu W, P_{BS} = 20W$.

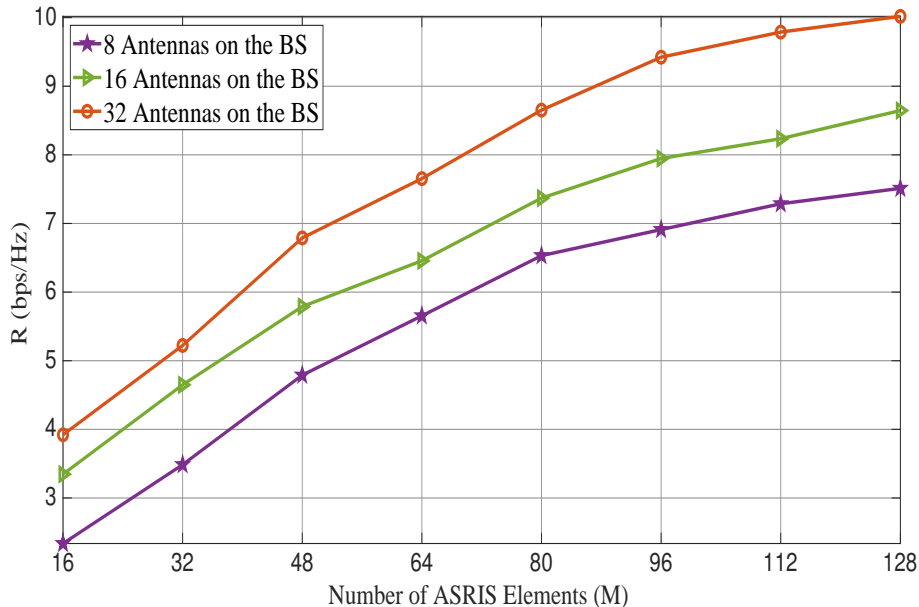


Fig. 6: Sum throughput maximization versus varying the number of elements in BS and ASRIS in the *PPO* method, with $I = 3, \varepsilon_{SBD_i} = 1\mu W$.

As illustrated in Fig. 6, increasing the number of elements in ASRIS from 16 to 128 exhibits a notable upward slope in the total data exchange rate. This phenomenon is attributed to more precise beamforming allocation and higher power for each of the SUEs. On the other hand, by augmenting the number of elements in BS from 8 to 32, the network's performance sees a significant improvement of approximately 133 percent. Consequently, users can engage in information exchange at a much higher rate compared to the previous rate. In this scenario, the cumulative data exchange rate can achieve 10 bps/Hz.

An noteworthy consideration in this scenario is the increase in the volume of information processing in the network, which amplifies the computational complexity and implementation challenges as the number of elements grows. Therefore, careful consideration must be given to determining an optimal number of elements.

Now, in light of the aforementioned details, for better comparison between these methods, we plot the graphs for the TD3 and A3C methods in the following figures.

As evident in Figs. 7 and 8, the data exchange rate in the A3C method is, on average under similar conditions, higher at 1 bps/Hz compared to the TD3 method. This scale holds approximately true for the TD3 graphs in comparison to the PPO ones as well.

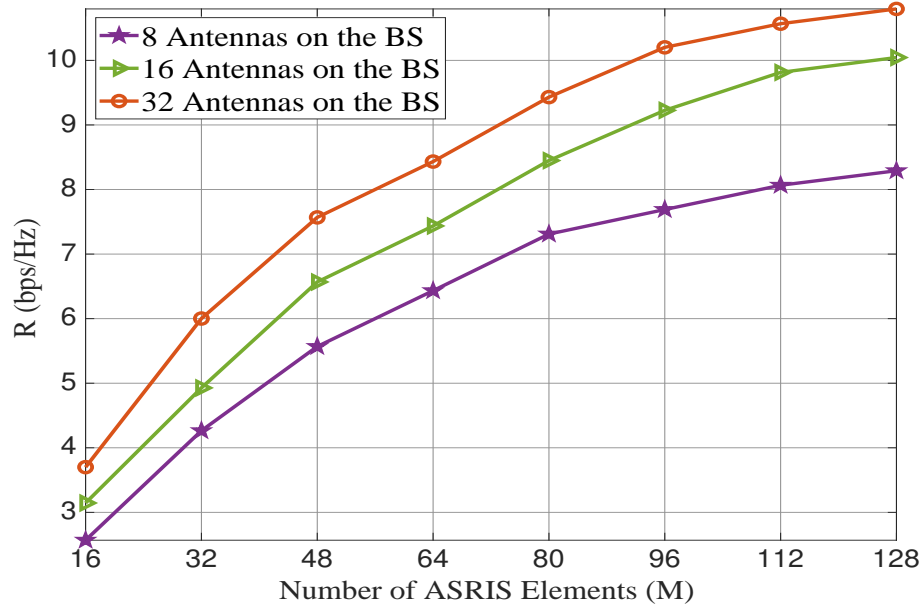


Fig. 7: Sum throughput maximization versus varying the number of elements in BS and ASRIS in the *TD3* method, with $I = 3, \varepsilon_{SBD_i} = 1\mu W$.

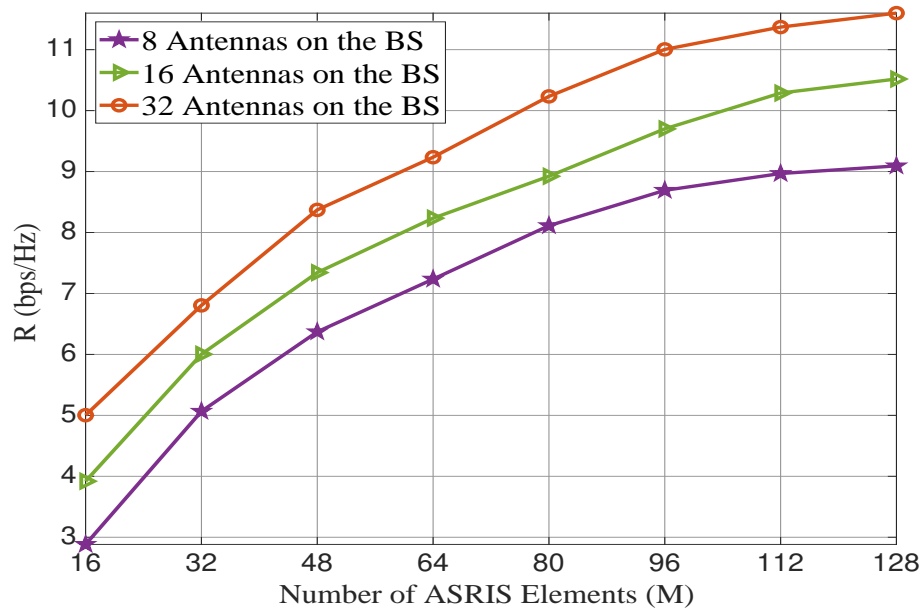


Fig. 8: Sum throughput maximization versus varying the number of elements in BS and ASRIS in the *A3C* method, with $I = 3, \varepsilon_{SBD_i} = 1\mu W$.

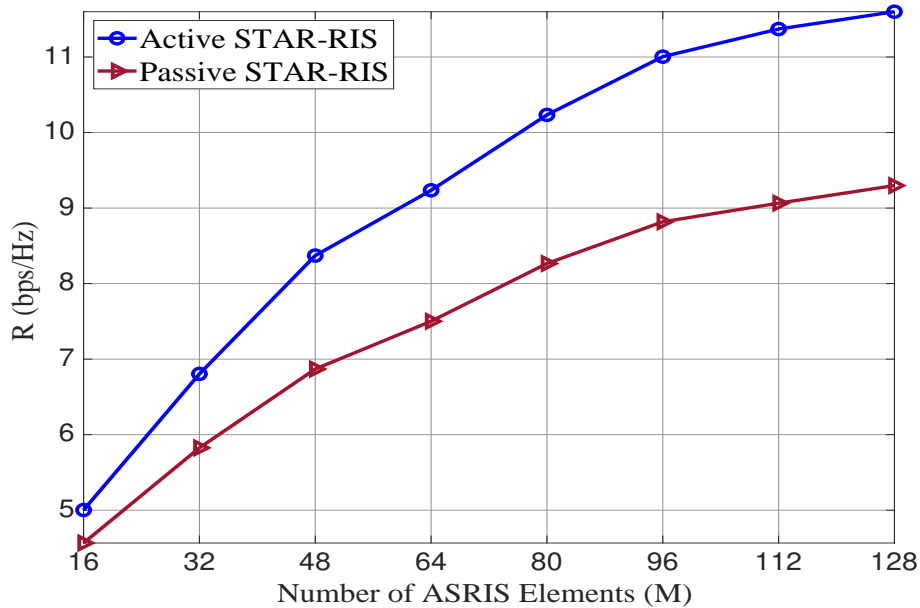


Fig. 9: Sum Throughput Maximization Versus the Number of Elements in Active and passive STAR-RIS in A3C method.

E. Comparison of Sum Throughput Maximization Versus the Number of Elements in Active and passive STAR-RIS

In the optimization problem 12 considered in the system model, we have included two constraints, 11b and 11c, corresponding to the modes involving passive and active STAR-RIS in the network, respectively. In this section, we aim to assess the efficacy of activating a STAR-RIS as opposed to its passive counterpart, as illustrated in Fig. 9.

As depicted in Fig. 9, the information exchange rate is almost 2 bps/Hz higher when actively employing STAR-RIS compared to the passive utilization of STAR-RIS. This value further increases with the addition of more elements to the STAR-RIS configuration.

VI. CONCLUSION AND FUTURE WORKS

In this article, we have explored a comprehensive system model incorporating various cutting-edge technologies, including Massive MIMO, ASRIS, and both passive and active users. The objective of this initiative is to achieve optimal resource allocation among users, aiming to maximize the sum throughput rate across the entire network. In this system, for a practical modeling approach, we have incorporated constraints to ensure the minimum required QoS, impose limits on the maximum power for both BS and ASRIS, account for the constraints on

the amount of energy harvesting for SBDs, and adhere to the requirements of satisfying SIC in the NOMA multiple access scheme. After mathematically modeling the target system, we encounter a non-convex and complex problem. To address the objectives inherent in this challenge, we leverage advanced DRL methods, including PPO, TD3, and A3C. The conducted simulations reveal that the A3C method, apart from achieving faster convergence, exhibits the capability to enhance the total throughput rate in the network when compared to the other two methods, TD3 and PPO. Additionally, the TD3 method significantly outperforms the PPO method. In the final segment of the simulation section, we draw the conclusion that the adoption of an active structure significantly influences the network throughput rate in comparison to the passive STAR-RIS mode.

To further advance this work, the inclusion of direct line-of-sight links between SBD and SUEs can be explored in addition to the current setup. Moreover, alternative DRL methods or a federated learning approach can be employed to model this problem.

REFERENCES

- [1] L. Chettri and R. Bera, "A comprehensive survey on internet of things (iot) toward 5g wireless systems," *IEEE Internet of Things Journal*, vol. 7, no. 1, pp. 16–32, 2020.
- [2] X. You, C.-X. Wang, J. Huang, X. Gao, Z. Zhang, M. Wang, Y. Huang, C. Zhang, Y. Jiang, J. Wang *et al.*, "Towards 6g wireless communication networks: Vision, enabling technologies, and new paradigm shifts," *Science China Information Sciences*, vol. 64, pp. 1–74, 2021.
- [3] Q. Wu, X. Zhou, W. Chen, J. Li, and X. Zhang, "Irs-aided wpcns: A new optimization framework for dynamic irs beamforming," *IEEE Transactions on Wireless Communications*, 2021.
- [4] K. Dev, P. K. R. Maddikunta, T. R. Gadekallu, S. Bhattacharya, P. Hegde, and S. Singh, "Energy optimization for green communication in iot using harris hawks optimization," *IEEE Transactions on Green Communications and Networking*, vol. 6, no. 2, pp. 685–694, 2022.
- [5] M. N. Mahdi, A. R. Ahmad, Q. S. Qassim, H. Natiq, M. A. Subhi, and M. Mahmoud, "From 5g to 6g technology: meets energy, internet-of-things and machine learning: a survey," *Applied Sciences*, vol. 11, no. 17, p. 8117, 2021.
- [6] L. Zhang, Y.-C. Liang, and D. Niyato, "6g visions: Mobile ultra-broadband, super internet-of-things, and artificial intelligence," *China Communications*, vol. 16, no. 8, pp. 1–14, 2019.
- [7] L. Zhang, Y.-C. Liang, and M. Xiao, "Spectrum sharing for internet of things: A survey," *IEEE Wireless Communications*, vol. 26, no. 3, pp. 132–139, 2018.
- [8] Z. Qin, X. Zhou, L. Zhang, Y. Gao, Y.-C. Liang, and G. Y. Li, "20 years of evolution from cognitive to intelligent communications," *IEEE transactions on cognitive communications and networking*, vol. 6, no. 1, pp. 6–20, 2019.
- [9] D. Samanta, C. K. De, and A. Chandra, "Performance analysis of full-duplex multi-relaying energy harvesting scheme in presence of multi-user cognitive radio network," *IEEE Transactions on Green Communications and Networking*, 2022.
- [10] V. Liu, A. Parks, V. Talla, S. Gollakota, D. Wetherall, and J. R. Smith, "Ambient backscatter: Wireless communication out of thin air," *ACM SIGCOMM computer communication review*, vol. 43, no. 4, pp. 39–50, 2013.
- [11] G. Yang, Q. Zhang, and Y.-C. Liang, "Cooperative ambient backscatter communications for green internet-of-things," *IEEE Internet of Things Journal*, vol. 5, no. 2, pp. 1116–1130, 2018.
- [12] M. B. Janjua and H. Arslan, "Survey on symbiotic radio: A paradigm shift in spectrum sharing and coexistence," *arXiv preprint arXiv:2111.08948*, 2021.
- [13] Z. Chen and B. Ji, "Resource allocation algorithm for iot communication based on ambient backscatter," in *2021 IEEE 93rd Vehicular Technology Conference (VTC2021-Spring)*. IEEE, 2021, pp. 1–5.
- [14] R. Long, Y.-C. Liang, H. Guo, G. Yang, and R. Zhang, "Symbiotic radio: A new communication paradigm for passive internet of things," *IEEE Internet of Things Journal*, vol. 7, no. 2, pp. 1350–1363, 2020.
- [15] Y.-C. Liang, Q. Zhang, E. G. Larsson, and G. Y. Li, "Symbiotic radio: Cognitive backscattering communications for future wireless networks," *IEEE Transactions on Cognitive Communications and Networking*, vol. 6, no. 4, pp. 1242–1255, 2020.
- [16] R. S. Yeganeh, M. J. Omid, and M. Ghavami, "Multi-bd symbiotic radio-aided 6g iot network: Energy consumption optimization with qos constraint approach," *IEEE Transactions on Green Communications and Networking*, 2023.
- [17] Q. Wu, S. Zhang, B. Zheng, C. You, and R. Zhang, "Intelligent reflecting surface-aided wireless communications: A tutorial," *IEEE Transactions on Communications*, vol. 69, no. 5, pp. 3313–3351, 2021.
- [18] Y. Liu, X. Mu, J. Xu, R. Schober, Y. Hao, H. V. Poor, and L. Hanzo, "Star: Simultaneous transmission and reflection for 360 coverage by intelligent surfaces," *IEEE Wireless Communications*, vol. 28, no. 6, pp. 102–109, 2021.
- [19] J. Xu, Y. Liu, X. Mu, and O. A. Dobre, "Star-riss: Simultaneous transmitting and reflecting reconfigurable intelligent surfaces," *IEEE Communications Letters*, vol. 25, no. 9, pp. 3134–3138, 2021.

- [20] H. Niu, Z. Chu, F. Zhou, P. Xiao, and N. Al-Dhahir, "Weighted sum rate optimization for star-ris-assisted mimo system," *IEEE transactions on vehicular technology*, vol. 71, no. 2, pp. 2122–2127, 2021.
- [21] X. Li, Y. Zheng, M. Zeng, Y. Liu, and O. A. Dobre, "Enhancing secrecy performance for star-ris noma networks," *IEEE Transactions on Vehicular Technology*, vol. 72, no. 2, pp. 2684–2688, 2022.
- [22] J. Xu, J. Zuo, J. T. Zhou, and Y. Liu, "Active simultaneously transmitting and reflecting (star)-riss: Modelling and analysis," *IEEE Communications Letters*, 2023.
- [23] R. Long, Y.-C. Liang, Y. Pei, and E. G. Larsson, "Active reconfigurable intelligent surface-aided wireless communications," *IEEE Transactions on Wireless Communications*, vol. 20, no. 8, pp. 4962–4975, 2021.
- [24] Z. Zhang, L. Dai, X. Chen, C. Liu, F. Yang, R. Schober, and H. V. Poor, "Active ris vs. passive ris: Which will prevail in 6g?" *IEEE Transactions on Communications*, vol. 71, no. 3, pp. 1707–1725, 2022.
- [25] J. Hu, Y.-C. Liang, Y. Pei, S. Sun, and R. Liu, "Reconfigurable intelligent surface based uplink mu-mimo symbiotic radio system," *IEEE Transactions on Wireless Communications*, vol. 22, no. 1, pp. 423–438, 2022.
- [26] J. Hu, Y.-C. Liang, and Y. Pei, "Reconfigurable intelligent surface enhanced multi-user miso symbiotic radio system," *IEEE Transactions on Communications*, vol. 69, no. 4, pp. 2359–2371, 2020.
- [27] J. Ye, S. Guo, S. Dang, B. Shihada, and M.-S. Alouini, "On the capacity of reconfigurable intelligent surface assisted mimo symbiotic communications," *IEEE Transactions on Wireless Communications*, vol. 21, no. 3, pp. 1943–1959, 2021.
- [28] C. Zhou, B. Lyu, Y. Feng, and D. T. Hoang, "Transmit power minimization for star-ris empowered symbiotic radio communications," *arXiv preprint arXiv:2304.10095*, 2023.
- [29] M. Wu, X. Lei, X. Zhou, X. Tang, and O. A. Dobre, "Ris-assisted energy-and spectrum-efficient symbiotic transmission in noma systems," *IEEE Transactions on Communications*, 2023.
- [30] X. Li, Q. Wang, M. Zeng, Y. Liu, S. Dang, T. A. Tsiftsis, and O. A. Dobre, "Physical-layer authentication for ambient backscatter-aided noma symbiotic systems," *IEEE Transactions on Communications*, vol. 71, no. 4, pp. 2288–2303, 2023.
- [31] H. Yang, H. Ding, M. El-kashlan, H. Li, and K. Xin, "A novel symbiotic backscatter-noma system," *IEEE Transactions on Vehicular Technology*, 2023.
- [32] S. Gong, X. Huang, J. Xu, W. Liu, P. Wang, and D. Niyato, "Backscatter relay communications powered by wireless energy beamforming," *IEEE Transactions on Communications*, vol. 66, no. 7, pp. 3187–3200, 2018.
- [33] J. Zuo, Y. Liu, Z. Ding, L. Song, and H. V. Poor, "Joint design for simultaneously transmitting and reflecting (star) ris assisted noma systems," *IEEE Transactions on Wireless Communications*, vol. 22, no. 1, pp. 611–626, 2022.
- [34] X. Mu, Y. Liu, L. Guo, J. Lin, and R. Schober, "Simultaneously transmitting and reflecting (star) ris aided wireless communications," *IEEE Transactions on Wireless Communications*, vol. 21, no. 5, pp. 3083–3098, 2021.
- [35] X. Zhai, G. Han, Y. Cai, Y. Liu, and L. Hanzo, "Simultaneously transmitting and reflecting (star) ris assisted over-the-air computation systems," *IEEE Transactions on Communications*, vol. 71, no. 3, pp. 1309–1322, 2023.
- [36] F. Zeinali, S. Norouzi, N. Mokari, and E. A. Jorswieck, "Ai-based radio resource and transmission opportunity allocation for 5g-v2x hetnets: Nr and nr-u networks," *International Journal of Electronics and Communication Engineering*, vol. 17, no. 9, pp. 217 – 224, 2023.
- [37] R. Zhang, K. Xiong, Y. Lu, P. Fan, D. W. K. Ng, and K. B. Letaief, "Energy efficiency maximization in ris-assisted swipt networks with rsma: A ppo-based approach," *IEEE Journal on Selected Areas in Communications*, vol. 41, no. 5, pp. 1413–1430, 2023.
- [38] L. Zhang, C. She, K. Ying, Y. Li, and B. Vucetic, "Deep reinforcement learning for improving resource utilization efficiency of urllc with imperfect channel state information," *IEEE Wireless Communications Letters*, vol. 12, no. 10, pp. 1796–1800, 2023.

- [39] J. Du, W. Cheng, G. Lu, H. Cao, X. Chu, Z. Zhang, and J. Wang, "Resource pricing and allocation in mec enabled blockchain systems: An a3c deep reinforcement learning approach," *IEEE Transactions on Network Science and Engineering*, vol. 9, no. 1, pp. 33–44, 2022.
- [40] M. Chen, T. Wang, K. Ota, M. Dong, M. Zhao, and A. Liu, "Intelligent resource allocation management for vehicles network: An a3c learning approach," *Computer Communications*, vol. 151, pp. 485–494, 2020.
- [41] R. K. Singh, P. P. Puluckul, R. Berkvens, and M. Weyn, "Energy consumption analysis of lpwan technologies and lifetime estimation for iot application," *Sensors*, vol. 20, no. 17, p. 4794, 2020.
- [42] J. Finnegan and S. Brown, "An analysis of the energy consumption of lpwa-based iot devices," in *2018 International Symposium on Networks, Computers and Communications (ISNCC)*. IEEE, 2018, pp. 1–6.
- [43] D. Poluektov, M. Polovov, P. Kharin, M. Stusek, K. Zeman, P. Masek, I. Gudkova, J. Hosek, and K. Samouylov, "On the performance of lorawan in smart city: End-device design and communication coverage," in *International Conference on Distributed Computer and Communication Networks*. Springer, 2019, pp. 15–29.
- [44] M. Lauridsen, R. Krigslund, M. Rohr, and G. Madueno, "An empirical nb-iot power consumption model for battery lifetime estimation," in *2018 IEEE 87th Vehicular Technology Conference (VTC Spring)*. IEEE, 2018, pp. 1–5.